Available online at www.sciencedirect.com
SCIENCE DIRECT®
Journal of Sound and Vibration 269 (2004) 33–60
JOURNAL OF SOUND AND VIBRATION
www.elsevier.com/locate/jsvi

Coupled bending, longitudinal and torsional vibrations of a cracked rotor

A.K. Darpe, K. Gupta*, A. Chawla

Department of Mechanical Engineering, Indian Institute of Technology, Hauz Khas, Delhi 110016, India

Received 16 May 2002; accepted 19 December 2002

Abstract

The coupling between longitudinal, lateral and torsional vibrations is studied together for a rotating cracked shaft. These coupling mechanisms have been studied here with a response-dependent non-linear breathing crack model. Most of the earlier work on coupled vibrations due to crack has been either on stationary shaft or on rotating shaft with open crack model. The stiffness matrix of a Timoshenko beam element is modified to account for the effect of a crack and all the six degrees of freedom per node are considered. Coupled torsional–longitudinal vibrations for a cracked rotor that has not been reported earlier and coupled torsional–bending vibrations with a breathing crack model have been studied. An attempt has been made to reveal crack specific signatures by using additional external excitations. Since all the couplings are accounted, the excitation in one mode leads to an interaction between all the modes. This, coupled with the rotational effect of a cracked rotor and the non-linearities due to a breathing crack model introduces sum and difference frequencies in the response of cracked rotor. The co-existence of frequencies of other modes in the frequency spectra of a particular mode and the presence of sum and difference frequencies around the excitation frequencies and its harmonics could be useful indicators for crack diagnosis.

1. Introduction

Fatigue cracks are a potential source of catastrophic failures in rotors. Researchers have put in considerable effort to develop a foolproof and reliable strategy to detect cracks in rotors. Twice the running frequency component and the subharmonic resonance at approximately half the bending critical speed of the rotor have been reported to be the two prominent crack indicators.

*Corresponding author. Tel.: +91-116-591122; fax: +91-116-851169.
E-mail address: kgupta@mech.iitd.ernet.in (K. Gupta).

0022-460X/03/$ - see front matter
doi:10.1016/S0022-460X(03)00003-8

Broadly, the efforts were made to first model the crack accounting for the reduction in the stiffness of the rotor segment, followed by modelling and use of stiffness variation in the equations of motion to estimate the rotor response. Dimarogonas and Papadopoulos [1] carried out analysis of cracked rotor neglecting the non-linear behaviour of the crack by assuming constant stiffness asymmetry and using theory of shafts with dissimilar moments of inertia. Later they derived a complete flexibility matrix of the cross-section containing the crack [2]. The flexibility matrix derived corresponds to a fully open crack. Later several researchers used this flexibility matrix to model a cracked rotor. The flexibility in rotor fixed direction was assumed to remain constant and thus equations of motion for cracked rotor were similar to an asymmetric shaft. To model the breathing of the crack, Grabowski [3] suggested switching of the stiffness values from those of an uncracked rotor (closed crack state) to those of cracked rotor (fully open state) at a particular rotor angular position (when crack edge becomes vertical). Alternatively the switching takes place when there is a change in the sign of rotor response in rotor fixed co-ordinate in crack direction (perpendicular to crack edge), which is referred as hinge model, introduced by Gasch [4] in 1976. Mayes and Davis [5] suggested sinusoidal stiffness variation to model the breathing in a more sensible way as a rotor crack is expected to open and close gradually due to gravity. Later Nelson and Nataraj [6] treated the finite element formulation of a crack element. They used rotating stiffness variation that depended on rotor curvature at crack section. Papadopoulos and Dimarogonas [7] represented stiffness variation by way of a truncated, four term series using known stiffness matrices corresponding to half open-half close, fully open and fully closed crack. Schmalhorst [8] used contact segments on the face of crack in a FE model to help decide which part of the crack face is under pressure and hence the breathing behaviour of the cracked part. Change et al. [9] represented the crack as a hinge with variable stiffness in two rotor-fixed lateral directions. The crack is introduced at a node of finite element model. The stiffness change is again dependent on direction of bending moment at the crack cross-section. Wauer [10] replaced the local geometric discontinuity by a discontinuity in load and used Galerkin's method to obtain response. The crack is assumed completely closed or completely open depending on the rotor curvature. Ostachowicz and Krawczuk [11] used finite element model with a modified stiffness matrix of beam accounting for the effect of crack and considering all but axial degree of freedom. They found lateral response to torsional excitation for a rotating shaft with open crack. Sekhar and Prabhu [12] used finite element model for the cracked rotor with open crack and studied possibility of backward whirl and fluctuation of bending stresses due to crack. Abraham and Brandon [13] proposed a substructure approach for modelling breathing behaviour of crack using Lagrange multipliers.

Papadopoulos and Dimarogonas [2,14–16] have extensively addressed the issue of coupling of vibrations due to crack. They proposed the presence of either of bending, longitudinal or torsional mode natural frequency in the vibration spectra of the other modes as a potential indicator of crack in the shaft. For this purpose they used harmonic sweeping excitation. The excitation, however, is given to non-rotating shaft. Ostachowicz and Krawczuk [11] demonstrated coupling of torsional and bending vibration in a rotating shaft using an open crack model. Muszynska et al. [17] discussed torsional/lateral vibration cross-coupled response due to shaft anisotropy. Presence of subharmonic torsional resonance is experimentally observed when rotational speed is at 1/8, 1/6, 1/4 and 1/2 of first torsional critical speed.

Collins et al. [18] and Darpe et al. [19] used impulse axial excitation to a rotating cracked shaft and exploited this coupling mechanism in lateral and longitudinal directions of a cracked rotor for the purpose of diagnosis of crack. Thus not only the natural frequency component but also the combination harmonics, due to interaction of rotational frequency and its harmonics with the constant excitation frequency and its harmonics, have been shown to appear in the spectrum [19]. Coupled flexural–torsional response of a cracked rotating shaft during passage through a critical speed has been investigated by Suherman and Plaut [20]. To the best of the author's knowledge, these studies [18–20] are the only one accounting for crack closing in case of coupled vibrations of cracked rotor.

Although a 6×6 flexibility matrix has been used in the analytical models of a non-rotating shaft by previous researchers for studying coupling, a finite element with all the six degrees of freedom accounting for all the coupling mechanisms has not been used to explore coupling of various modes in a rotating shaft. Most of the previous work that addressed the coupling has been on stationary (non-rotating) shaft [14–16]. Those who addressed the issue of coupling in a rotating cracked shaft either used only one coupling (bending–longitudinal [2,17,18] and torsional–bending [11]) or used open crack model [2,11]. An open crack model is an unrealistic model and can give different results from those obtained with a more appropriate breathing crack model. The work of Papadopoulos and Dimarogonas [16] is the only one that studied coupling between all the three modes of vibration, although it was for a non-rotating shaft with open crack. Papadopoulos and Dimarogonas [14,15] have emphasized the need for further analysis with non-linear effects of breathing crack model for rotating shafts. To the best of authors information, the torsional–axial vibrations for a cracked rotor has not been yet studied.

In this paper an attempt is made to address some of the issues mentioned above. The work presented accounts for coupling between longitudinal, lateral and torsional vibrations for a rotating cracked shaft using a response-dependent non-linear breathing crack model. The stiffness matrix of a beam element is modified to account for the effect of a crack and all the six degrees of freedom per node are considered. By including the axial degree of freedom in the present analysis, the stiffness matrix formulated is an extension of the one developed by Ostachowicz and Krawczuk [11]. This has made possible the analysis of coupling of longitudinal vibrations with bending and torsional vibrations of a cracked rotating shaft. In addition, a refined breathing crack model that accounts for partial opening/closing of crack through sign of stress intensity factor at the crack edge is used.

2. Finite element model of a cracked rotor segment

Consider a rotor segment containing a single transverse surface crack. To represent this segment in the finite element model of the cracked rotor system, the rotor segment is represented by a beam element with six degrees of freedom per node. However, to account for the presence of a crack, the stiffness matrix of the beam element is modified. The modified stiffness matrix takes into account all the coupling phenomena that exists in a cracked rotor, i.e., bending–longitudinal, bending–torsion, longitudinal–torsion. The beam element with modified stiffness matrix then fits into the complete finite element assemblage representing a rotor–bearing system and is used for further analysis.

Consider a shaft element containing a transverse surface crack of depth a as shown in Fig. 1. A small shaft segment around the crack cross-section in the rotor will be modelled as a finite beam element that will be different than the usual beam element with regard to its stiffness properties. Let the shaft element be of diameter D and length l. The element is loaded with shear forces P_2, P_3 and P_8, P_9, bending moments P_4, P_5 and P_{11}, P_{12}, axial forces P_1 and P_7 and torsional moments

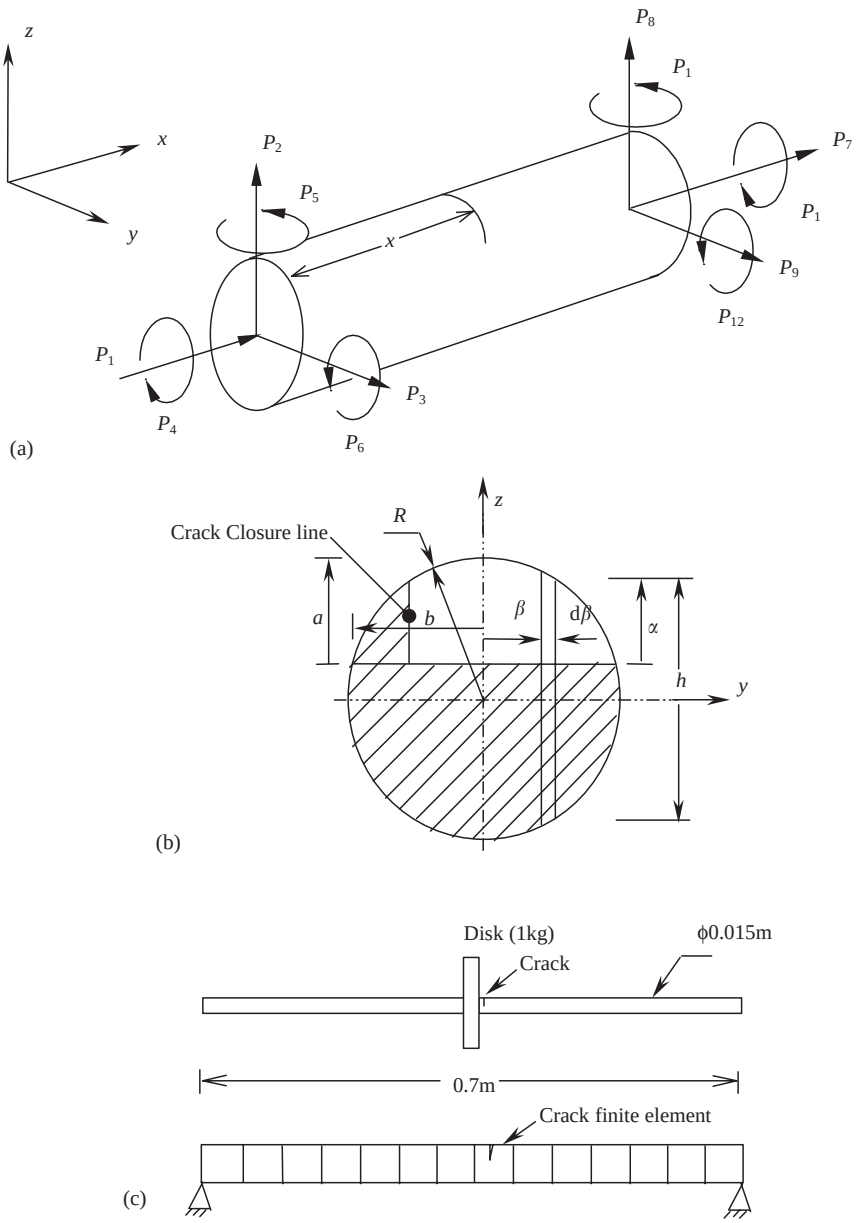

Fig. 1. Shaft finite element. (a) The element showing forces acting and co-ordinate system. (b) Crack cross-section. (c) A simple rotor and its finite element model.

P_4 and P_{10}. Thus, all the six degrees of freedom per node is considered here. The crack is situated at a distance x from the left end of the element.

The flexibility matrix of the crack element is first derived. Using Castingliano's theorem,

$$u_i = \frac{\partial U}{\partial P_i}, \tag{1}$$

where U is the total strain energy. That is,

$$U = U^0 + U^c. \tag{2}$$

Here, U^0 is the strain energy of the uncracked shaft element; U^c the strain energy due to crack

Let u_i and P_i are displacement and force respectively along the ith co-ordinate. Thus,

$$u_i = \frac{\partial U^0}{\partial P_i} + \frac{\partial U^c}{\partial P_i}$$

which can be written as

$$u_i = u_i^0 + u_i^c, \tag{3}$$

where

$$u_i^0 = \frac{\partial U^0}{\partial P_i}, \quad u_i^c = \frac{\partial U^c}{\partial P_i}. \tag{4}$$

Using the strain energy approach, both u_i^0 and u_i^c will be derived. Considering the action of axial forces, torsion and bending moments and also accounting for shearing action at the cross-section of the crack the elastic strain energy of the element can be written as

$$U^0 = \frac{1}{2}\int \left[\frac{\alpha_s V_1^2}{GA} + \frac{\alpha_s V_2^2}{GA} + \frac{M_1^2}{EI} + \frac{M_2^2}{EI} + \frac{T^2}{GI_0} + \frac{F^2}{AE}\right] \mathrm{d}x \tag{5}$$

where V_1, V_2 are shear forces, M_1, M_2 are bending moments, T is torsional moment, F is the axial force acting at the crack cross-section, G is modulus of rigidity, E is Young's modulus, I is the area moment of inertia of the cross-section, I_0 is the polar moment of inertia of the cross-section and α_s is the shear coefficient.

From Fig. 1,

$$V_1 = P_2, \quad V_2 = P_3, \quad T = P_4, \quad F = P_1, \quad M_1 = P_2 x - P_6 \quad \text{and} \quad M_2 = P_3 x + P_5. \tag{6}$$

Thus, Eq. (5) now becomes,

$$U^0 = \frac{1}{2}\left[\frac{P_1^2 l}{AE} + \frac{\alpha_s P_2^2 l}{GA} + \frac{P_2^2 l^3}{3EI} + \frac{\alpha_s P_3^2 l}{GA} + \frac{P_3^2 l^3}{3EI} + \frac{P_4^2 l}{GI_0} + \frac{P_5^2 l}{EI} + \frac{P_6^2 l}{EI} - \frac{P_2 P_6 l^2}{EI} + \frac{P_3 P_5 l^2}{EI}\right]. \tag{7}$$

Now the individual displacements u_i^0 can be written as

$$u_1^0 = \frac{\partial U^0}{\partial P_1} = \frac{\mathrm{d}}{\mathrm{d}P_1}\left[\frac{1}{2}\frac{P_1^2 l}{AE}\right],$$

$$u_1^0 = \frac{P_1 l}{AE}. \tag{8}$$

Similarly

$$u_2^0 = \frac{\partial U^0}{\partial P_2} = \frac{\mathrm{d}}{\mathrm{d}P_2}\left[\frac{1}{2}\left(\frac{\alpha_s P_2^2 l}{GA} + \frac{P_2^2 l^3}{3EI}\right) - \frac{1}{2}\frac{P_2 P_6 l^2}{EI}\right],$$

$$u_2^0 = \left(\frac{\alpha_s l}{GA} + \frac{l^3}{3EI}\right)P_2 - \frac{l^2}{2EI}P_6. \tag{9}$$

Following similar procedure we get

$$u_3^0 = \left(\frac{\alpha_s l}{GA} + \frac{l^3}{3EI}\right)P_3 + \frac{l^2}{2EI}P_5, \tag{10}$$

$$u_4^0 = \frac{l}{GI_0}P_4, \tag{11}$$

$$u_5^0 = \frac{l}{EI}P_5 + \frac{l^2}{2EI}P_3, \tag{12}$$

$$u_6^0 = \frac{l}{EI}P_6 - \frac{l^2}{2EI}P_2. \tag{13}$$

The displacements u_i^0 using elastic strain energy of uncracked shaft element has been obtained. Now additional displacements u_i^c due to crack can be found using strain energy due to crack as follows:

$$u_i^c = \frac{\partial U^c}{\partial P_i},$$

where U^c is the strain energy due to the presence of crack, u_i^c, P_i are additional displacement and load in direction i due to crack.

Using concepts of fracture mechanics, the additional strain energy due to crack is given by the following expression:

$$U^c = \int_A J(A)\,\mathrm{d}A, \tag{14}$$

where $J(A)$ is strain energy density function and is expressed as

$$J(A) = \frac{1}{E'}\left[\left(\sum_{i=1}^{6} K_{\mathrm{I}i}\right)^2 + \left(\sum_{i=1}^{6} K_{\mathrm{II}i}\right)^2 + m\left(\sum_{i=1}^{6} K_{\mathrm{III}i}\right)^2\right]. \tag{15}$$

Here $E' = E/(1-v)$ and $m = 1+v$; v is the Poisson ratio and $K_{\mathrm{I}i}$ is the stress intensity factors corresponding to the opening mode of crack displacement, $K_{\mathrm{II}i}$ is the stress intensity factors corresponding to the sliding mode of crack displacement and $K_{\mathrm{III}i}$ is the stress intensity factors corresponding to the shearing mode of crack displacement; $i = 1-6$.

These stress intensity factors (SIF) are given as follows:

SIF for Mode I:

$$K_{\mathrm{I}1} = \sigma_1\sqrt{\pi\alpha}F_1(\alpha/h),$$

$$\sigma_1 = \frac{P_1}{\pi R^2}.$$

Hence

$$K_{I1} = \frac{P_1}{\pi R^2}\sqrt{\pi\alpha}F_1(\alpha/h), \tag{16}$$

$$K_{I5} = \sigma_5\sqrt{\pi\alpha}F_1(\alpha/h),$$
$$\sigma_5 = \frac{M_2\beta}{\pi/64\mathrm{D}^4},$$

and moment $M_2 = (P_5 + P_3x)$.

Hence,

$$K_{I5} = \frac{4(P_5 + P_3x)\beta}{\pi R^4}\sqrt{\pi\alpha}F_1(\alpha/h), \tag{17}$$

$$K_{I6} = \sigma_6\sqrt{\pi\alpha}F_2(\alpha/h),$$
$$\sigma_6 = \frac{M_1\sqrt{R^2-\beta^2}}{\pi/64\mathrm{D}^4},$$

and moment $M_1 = (P_2x - P_6)$,

$$K_{I6} = \frac{2(P_2x - P_6)h}{\pi R^4}\sqrt{\pi\alpha}F_2(\alpha/h), \tag{18}$$

$$K_{I2} = K_{I3} = K_{I4} = 0. \tag{19}$$

SIF for Mode II:

$$K_{II2} = \sigma_2\sqrt{\pi\alpha}F_{II}(\alpha/h),$$
$$\sigma_2 = \frac{kP_2}{\pi R^2}.$$

Hence,

$$K_{II2} = \frac{kP_2}{\pi R^2}\sqrt{\pi\alpha}F_{II}(\alpha/h), \tag{20}$$

$$K_{II4} = \sigma_{4II}\sqrt{\pi\alpha}F_{II}(\alpha/h),$$
$$\sigma_{4II} = \frac{P_4\beta}{\pi/32D^4}.$$

Hence,

$$K_{II4} = \frac{2P_4\beta}{\pi R^4}\sqrt{\pi\alpha}F_{II}(\alpha/h), \tag{21}$$

$$K_{II1} = K_{II3} = K_{II5} = K_{II6} = 0. \tag{22}$$

SIF for Mode III:

$$K_{III3} = \sigma_3 \sqrt{\pi\alpha} F_{III}(\alpha/h),$$
$$\sigma_3 = \frac{kP_3}{\pi R^2}.$$

Hence,

$$K_{III3} = \frac{kP_3}{\pi R^2} \sqrt{\pi\alpha} F_{III}(\alpha/h), \tag{23}$$

$$K_{III4} = \sigma_{4III} \sqrt{\pi\alpha} F_{III}(\alpha/h),$$
$$\sigma_{4III} = \frac{P_4 \sqrt{R^2 - \beta^2}}{\pi/32D^4}.$$

Hence,

$$K_{III4} = \frac{P_4 h}{\pi R^4} \sqrt{\pi\alpha} F_{III}(\alpha/h), \tag{24}$$

$$K_{III1} = K_{III2} = K_{III5} = K_{III6} = 0,$$

where,

$$F_1 = \sqrt{\frac{2\alpha'}{\pi\alpha'} \tan\left(\frac{\pi\alpha}{2\alpha'}\right)} \frac{0.752 + 2.02(\alpha/\alpha') + 0.37[1 - \sin(\pi\alpha/2\alpha')]^3}{\cos\left(\pi\alpha/2\alpha'\right)},$$
$$F_2 = \sqrt{\frac{2\alpha'}{\pi\alpha} \tan\left(\frac{\pi\alpha}{2\alpha'}\right)} \frac{0.923 + 0.199[1 - \sin(\pi\alpha/2\alpha')]^4}{\cos(\pi\alpha/2\alpha')},$$
$$F_{II} = \frac{1.122 - 0.561(\alpha/\alpha') + 0.085(\alpha/\alpha')^2 + 0.18(\alpha/\alpha')^3}{\sqrt{1 - (\alpha/\alpha')}},$$
$$F_{III} = \sqrt{\frac{2\alpha'}{\pi\alpha} \tan\left(\frac{\pi\alpha}{2\alpha'}\right)}.$$

Using these SIF expressions in Eq. (15) and using $J(A)$ in Eq. (14), we get

$$u_1^c = [P_1 I_{g1} + (xP_2 - P_6) I_{g2} + (xP_3 + P_5) I_{g3}],$$
$$u_2^c = [xI_{g2} P_1 + I_{g4} P_2 + (xP_2 - P_6) xI_{g5} + (xP_3 + P_5) xI_{g6} + I_{g7} P_4],$$
$$u_3^c = [xI_{g3} P_1 + I_{g10} P_4 + (xP_2 - P_6) xI_{g6} + (xP_3 + P_5) xI_{g8} + I_{g9} P_3],$$
$$u_4^c = [R^2 I_{g7} P_2 + I_{g10} P_3 + (I_{g11} + I_{g12}) P_4],$$
$$u_5^c = [I_{g3} P_1 + (xP_2 - P_{6,}) I_{g6} + (xP_3 + P_5) I_{g8}],$$
$$u_6^c = [-I_{g2} P_1 - (xP_2 - P_6) I_{g5} - (xP_3 + P_5) I_{g6}],$$

where

$$I_{g1}=\int_A \frac{2\alpha F_{\mathrm{I}}^2}{\pi E R^4}\mathrm{d}A,\quad I_{g2}=\int_A \frac{4h\alpha F_1F_2}{\pi E R^6}\mathrm{d}A,\quad I_{g3}=\int_A \frac{8\beta\alpha F_{\mathrm{I}}^2}{\pi E R^6}\mathrm{d}A,$$
$$I_{g4}=\int_A \frac{2k^2\alpha F_{\mathrm{II}}^2}{\pi E R^4}\mathrm{d}A,\quad I_{g5}=\int_A \frac{8h^2\alpha F_2^2}{\pi E R^8}\mathrm{d}A,\quad I_{g6}=\int_A \frac{16h\beta\alpha F_1F_2}{\pi E R^8}\mathrm{d}A,$$
$$I_{g7}=\int_A \frac{4k\alpha\beta F_{\mathrm{II}}^2}{\pi E R^8}\mathrm{d}A,\quad I_{g8}=\int_A \frac{32\beta^2\alpha F_{\mathrm{I}}^2}{\pi E R^8}\mathrm{d}A,\quad I_{g9}=\int_A \frac{2mk^2\alpha F_{\mathrm{III}}^2}{\pi E R^4}\mathrm{d}A,$$
$$I_{g10}=\int_A \frac{2mkh\alpha F_{\mathrm{III}}^2}{\pi E R^6}\mathrm{d}A,\quad I_{g11}=\int_A \frac{8\beta^2\alpha F_{\mathrm{II}}^2}{\pi E R^8}\mathrm{d}A,\quad I_{g12}=\int_A \frac{2mh^2\alpha F_{\mathrm{III}}^2}{\pi E R^8}\mathrm{d}A. \tag{25}$$

Thus the total displacement u_i can now be obtained by adding u_i^0 to u_i^c (Eq. (3)) using Eqs. (8)–(13) and (25). The resulting equation can be written in matrix form as

$$u_i=[G]P_i,\quad i=1-6. \tag{26}$$

Here G is a flexibility matrix given by

$$G=\begin{bmatrix} g_{11} & g_{12} & g_{13} & g_{14} & g_{15} & g_{16}\\ g_{21} & g_{22} & g_{23} & g_{24} & g_{25} & g_{26}\\ g_{31} & g_{32} & g_{33} & g_{34} & g_{35} & g_{36}\\ g_{41} & g_{42} & g_{43} & g_{44} & g_{45} & g_{46}\\ g_{51} & g_{52} & g_{53} & g_{54} & g_{55} & g_{56}\\ g_{61} & g_{62} & g_{63} & g_{64} & g_{65} & g_{66} \end{bmatrix}, \tag{27}$$

where

$$g_{11}=\frac{l}{AE}+I_{g1},\quad g_{22}=\left(\frac{\alpha_s l}{GA}+\frac{l^3}{3EI}\right)+(I_{g4}+x^2I_{g5}),\quad g_{33}=\left(\frac{\alpha_s l}{GA}+\frac{l^3}{3EI}\right)+(I_{g9}+x^2I_{g8}),$$
$$g_{44}=\frac{l}{GI_0}+I_{g11}+I_{g12},\quad g_{55}=\frac{l}{EI}+I_{g8},\quad g_{66}=\frac{l}{EI}+I_{g5},\quad g_{12}=g_{21}=xI_{g2},$$
$$g_{13}=g_{31}=xI_{g3},\quad g_{15}=g_{51}=I_{g3},\quad g_{16}=g_{61}=-I_{g2},\quad g_{23}=g_{32}=x^2I_{g6},$$
$$g_{24}=g_{42}=R^2I_{g7},\quad g_{34}=g_{43}=I_{g10},\quad g_{25}=g_{52}=xI_{g6},\quad g_{35}=g_{53}=\frac{l^2}{2EI}+xI_{g8},$$
$$g_{26}=g_{62}=-\frac{l^2}{2EI}-xI_{g5},\quad g_{36}=g_{63}=-xI_{g6},\quad g_{56}=g_{65}=-I_{g6}. \tag{28}$$

The flexibility matrix is now used to find the stiffness matrix using the transformation matrix T considering static equilibrium of the finite element.

$$\{q_{1-12}\}^{\mathrm{T}}=[T]\{q_{1-6}\}^{\mathrm{T}}, \tag{29}$$

where the transformation matrix is given by

$$[T]^{\mathrm{T}} = \begin{bmatrix} 1 & 0 & 0 & 0 & 0 & 0 & -1 & 0 & 0 & 0 & 0 & 0 \\ 0 & 1 & 0 & 0 & 0 & 0 & 0 & -1 & 0 & 0 & 0 & l \\ 0 & 0 & 1 & 0 & 0 & 0 & 0 & 0 & -1 & 0 & -l & 0 \\ 0 & 0 & 0 & 1 & 0 & 0 & 0 & 0 & 0 & -1 & 0 & 0 \\ 0 & 0 & 0 & 0 & 1 & 0 & 0 & 0 & 0 & 0 & -1 & 0 \\ 0 & 0 & 0 & 0 & 0 & 1 & 0 & 0 & 0 & 0 & 0 & -1 \end{bmatrix}. \tag{30}$$

Thus, the stiffness matrix of the crack element is written as

$$[K]^{c} = [T][G][T]^{\mathrm{T}}. \tag{31}$$

3. Modelling of breathing behaviour of crack

When the rotor is operating at a steady state speed far away from critical speed and without any transient excitation, the breathing of the crack can be approximated either by sinusoidal stiffness variation or by stepwise stiffness fluctuation. However, a truly breathing behaviour can be represented by taking into account the gradual opening and closing of the crack using the stress intensity factor at the crack front at each instant and then finding the amount of crack opening and hence the stiffness. In this way, apart from getting a more accurate estimation of stiffness and more realistic representation of breathing, the model would be adaptable for all speed ranges and all type of excitations, steady as well as transient.

The integration limits for the evaluation of the flexibility coefficients using Eq. (28) are to be taken for full width from $-b$ to b (b is half-width of the crack (Fig. 1b)) and for full depth from 0 to a if the crack is fully open. Papadopoulos and Dimarogonas [2] and later mostly other researchers found the local flexibility assuming the fully open crack. Using these flexibility values corresponding to fully open crack, the stiffness variation is expressed in various ways as mentioned earlier in Section 1. However, since in practice the crack breathes, opening gradually from fully closed to fully open state and thereafter closes gradually to fully closed state from the fully open condition, proper integration limits need to be considered to evaluate stiffness values. These limits depend on the amount of crack opening [6]. For fully open crack the limits can be taken from $-b$ to b, whereas for half open half closed crack these limits would be either from 0 to b or from $-b$ to 0 depending upon which half of the crack is open.

To be able to study the flexibility variation with amount of crack opening, a concept of crack closure line (CCL) is proposed. The crack closure line is an imaginary line perpendicular to the crack edge. It separates the open and closed parts of the crack as illustrated in Fig. 2. The crack edge is divided into 50 points in the present case. The position of CCL keeps changing along the crack edge (say from 1 to 50 while opening from B to A and from 50 to 100 while closing from B to A) as the rotor rotates clockwise. When the rotor is at initial position (Fig. 2a), the crack edge is on the compression region and is closed completely under the action of gravity. As the rotor starts rotating clockwise, part of the crack near end 'B' opens up. The crack edge opens fully when it comes on the lower side in the tensile region at $\theta = 180^{\circ}$ (Fig. 2e). At this position the CCL has

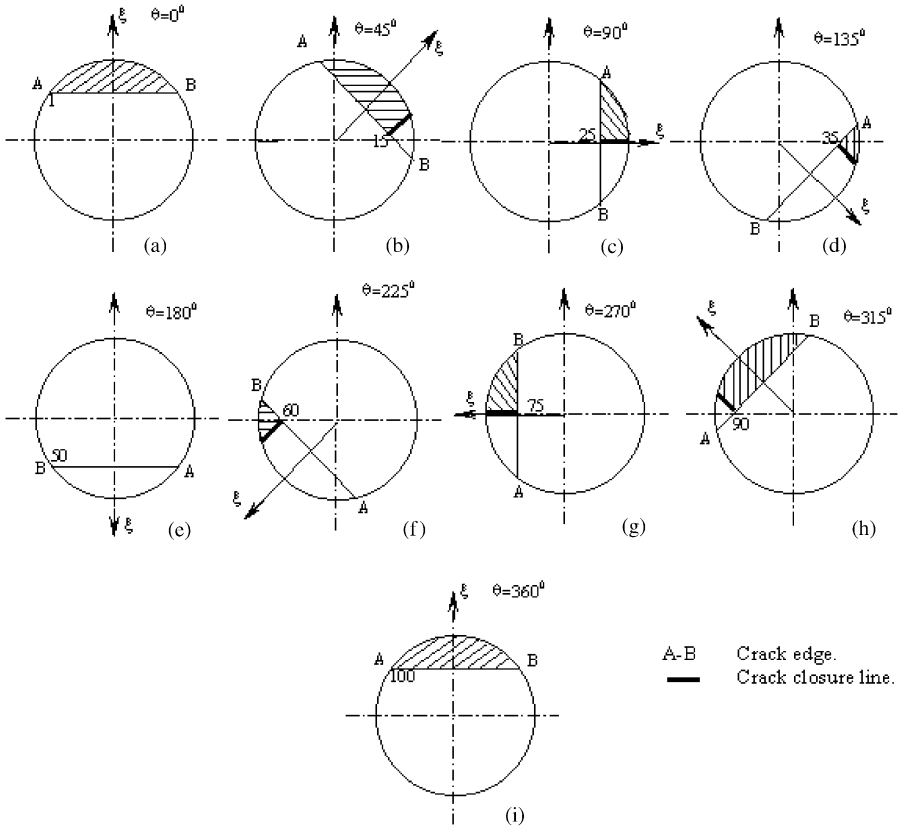

Fig. 2. Variation of crack closure line position with angular position of rotor.

travelled from one corner B to the other corner A. When the rotor rotates further the corner B starts to close till the crack completely closes at $\theta = 360°$. Thus the CCL positions (CCLP) of 1 and 100 indicate fully closed crack state, whereas CCLP of 50 indicates fully open crack state. CCLP of 25 indicates half open–half closed condition (right half open) and CCLP of 75 indicates half closed–half open condition (left half open) of the crack. Thus the continuous change of CCLP is indicative of breathing of the crack.

The variation of various flexibility coefficients as a function of crack closure line position is shown in Fig. 3. The flexibility coefficients are found for a crack finite element of diameter $d = 0.015$ and length of $L = 0.05$ with a crack of depth $\bar{a} = 0.4$. All the direct flexibility coefficients (g_{11}, g_{22}, g_{33}, g_{44}, g_{55} and g_{66}) increase to a maximum when the crack fully opens (near CCLP of 50). However, some of the cross-coupled flexibility coefficients (g_{13}, g_{15}, g_{23}, g_{24}, g_{25}, g_{36} and g_{56}) are zero when the crack fully opens. These coefficients have been earlier reported to be non-zero because the integration therein has been carried out from 0 to b followed by doubling the resulting integral value [2]. However, the value of the integral from 0 to b and that obtained from $-b$ to 0 is of same numerical value but have opposite sign. It may also be noted that the flexibility coefficient g_{35} and g_{26} are non-zero at fully closed state and they increase in magnitude as the crack opens.

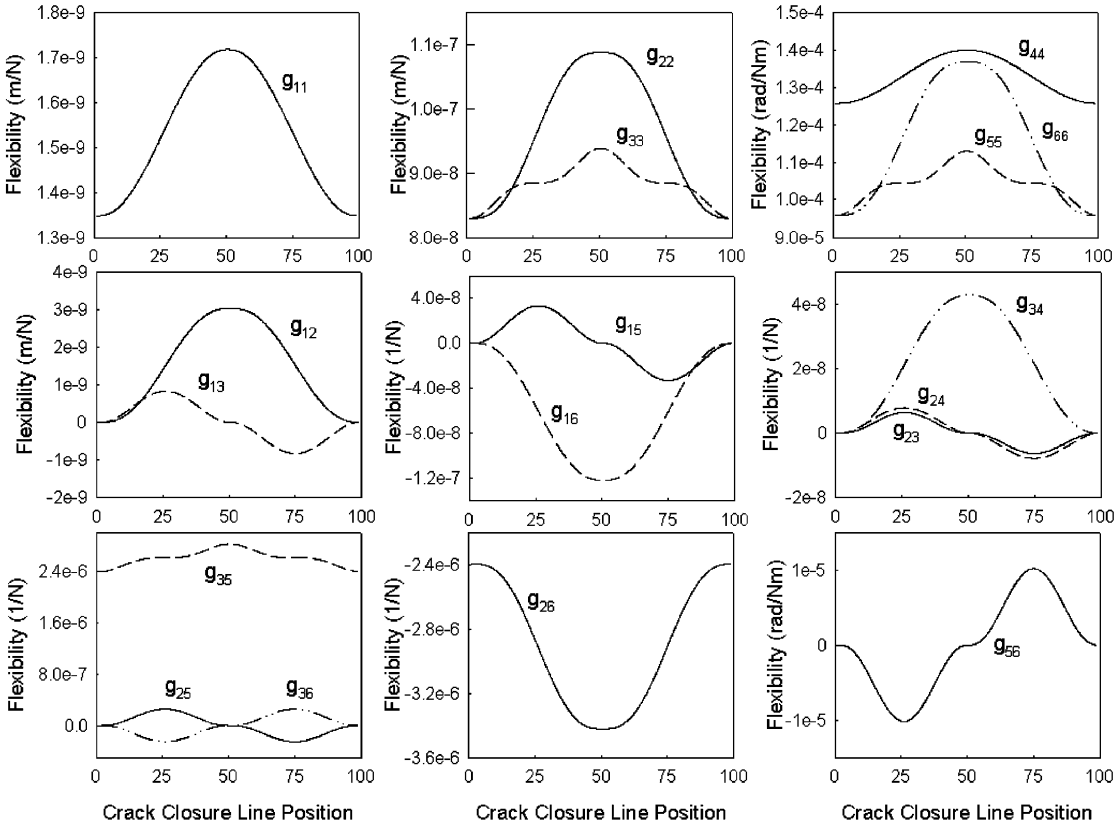

Fig. 3. Variation of flexibility coefficients for different amount of crack opening for a crack element with $\bar{a} = 0.4$, $l = 0.05$ and $d = 0.015$.

The variation of stiffness coefficients obtained from Eq. (31) with respect to crack closure line position is shown in Fig. 4. As the crack gradually opens, all the stiffness values drop from those corresponding to uncracked shaft element till they become minimum at the fully open crack position (CCLP = 50). The stiffness variation is not quite noticeable for shallow depths of $\bar{a} = 0.1$ but is substantial for deeper crack ($\bar{a} > 0.2$). The drop in stiffness with crack depth is clearly non-linear. Thus, we find that the crack breathing behaviour has significant influence on the variation of stiffness coefficients.

The calculation of stiffness of crack element and the response estimation are interdependent. This is because the response is dependent on the stiffness values used in the equation of motion and stiffness values are estimated from the response using the sign of SIF values. The equation of motion in stationary co-ordinates is

$$[M]^s\{\ddot{q}\}^s + [C]^s\{\dot{q}\}^s + [K]^s\{q\}^s = \{f\}^s, \tag{32}$$

where $[M]^s$, $[C]^s$ and $[K]^s$ are mass, damping and stiffness matrices for the rotor system in stationary co-ordinate system. Of these, only stiffness matrix is constantly updated, usually after every degree of rotation, as it is assumed response dependent. Scheme of updating the stiffness

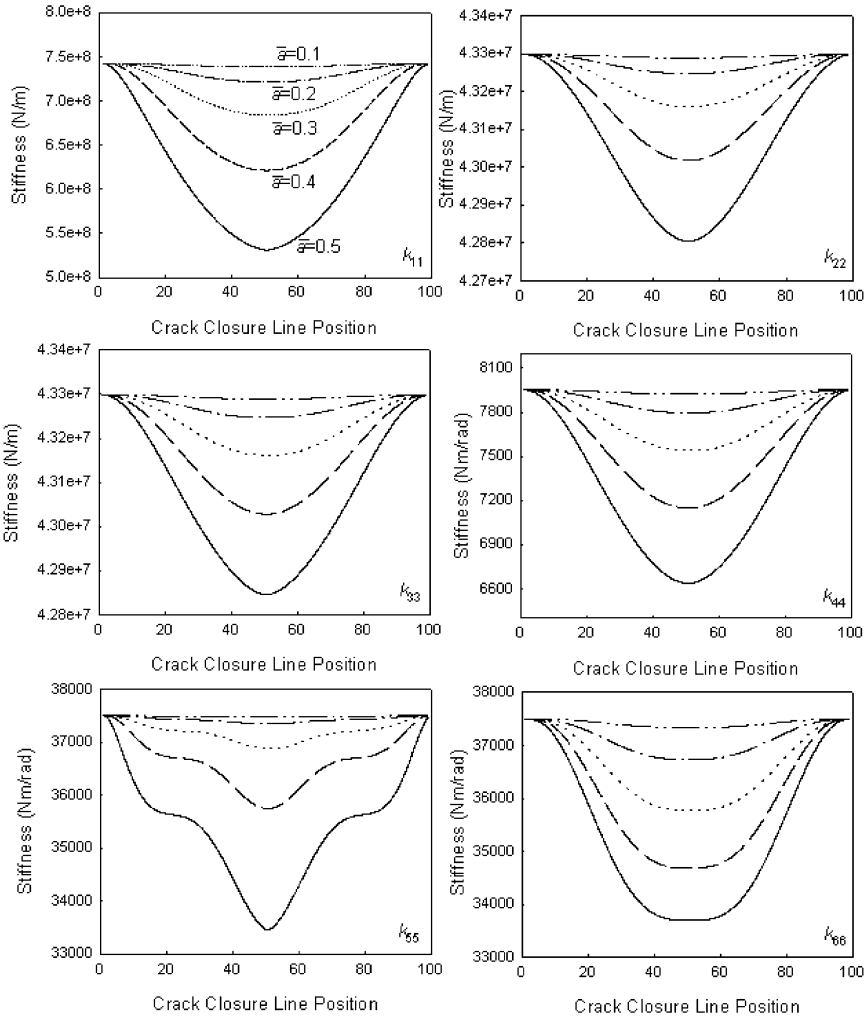

Fig. 4. Variation of various stiffness coefficients with amount of crack opening for different crack depth ratios ($d=0.015$, $l=0.05$).

matrix is discussed in the following paragraph. The mass and damping matrices are assumed constant. Proportional damping matrix is assumed here with $[C]^s = \alpha_d[K_{uc}] + \beta_d[M]$, where the constants α_d and β_d are assumed equal to 0.8132 and 1.3623e-5 respectively. These constants are evaluated based on the assumption of modal damping ratios of 0.005 and 0.01 in first two modes of the uncracked rotor system. $[K_{uc}]$ is the stiffness matrix without crack. The force vector $\{f\}^s$ contains gravity and unbalance excitation forces. If applied, torsional excitation terms also appear in the force vector. In the Newmark method of direct integration of equations of motion, integration parameters $\alpha_i=0.25$ and $\delta_i=0.5$ [21] are used to estimate the response of the rotor. The integration time step Δt is assumed to be 1/50th of the time required for a degree of rotation, which even for a slow speed of 22 rad/s is sufficiently small (1.5867e-5 s). Since the axial vibrations are studied, the sampling frequency with this integration time step is more than 63 000 Hz, which

is sufficient to track even the natural frequency of longitudinal vibrations (1150 Hz). Finer time step has not shown any influence on the response.

To evaluate the response, an initial assumed response vector $\{q\}^{s}$ corresponding to the static deflection of the uncracked rotor and initial stiffness matrix $[K]^{s}$, corresponding to the stiffness of the uncracked rotor is assumed. The equations are solved in the stationary co-ordinate system. The integration is carried out for time equal to a degree of rotation during which stiffness matrix is assumed constant. After every degree of rotation the stiffness matrix $[K]^{s}$ needs to be updated to take care of the breathing behaviour of the cracked rotor. For this purpose, the forces on the crack edge need to be evaluated in the rotor-fixed-co-ordinates. Hence, the new response vector $\{q\}^{s}$ obtained from the integration of Eq. (32) is used to find the response in the rotor-fixed co-ordinates $\{q\}^{r}$ using an appropriate co-ordinate transformation matrix, $\boldsymbol{T_g}$ [21]. The nodal forces are then calculated as

$$[P] = [K]^{r}\{q\}^{r}. \tag{33}$$

The above nodal forces are used to find the SIF along the crack edge. The nodal forces are used in Eqs. (16)–(18) to evaluate stress intensity factors. Overall value of SIF (K^{0}) at 50 equally spaced points along the crack edge is evaluated using following relation:

$$K^{0} = K_{I1} + K_{I5} + K_{I6}. \tag{34}$$

In the above equation only K_{I1}, K_{I5}, K_{I6} are accounted for as they are responsible for opening mode crack displacement. A negative sign of overall SIF at any point along crack edge indicates compressive stress at that point and hence the crack is assumed closed there. Similarly positive sign of SIF indicates tensile stress and the open state of crack. Thus the position along the crack edge where SIF changes its sign is the crack closure line position (CCLP). Once the CCLP is ascertained, the flexibility values are found by applying appropriate integration limits in Eq. (25). Once the 6×6-flexibility matrix is obtained using Eq. (28) the corresponding stiffness matrix for the crack element is obtained from Eq. (31) as discussed in the previous section and the global stiffness matrix can be assembled. However, the stiffness matrix obtained is in rotor-fixed co-ordinates and for transforming the matrix from the rotor fixed to the stationary co-ordinates, the global transformation matrix $[T_g]$ is assembled using the elemental co-ordinate transformation matrix $[T_e]$ given by

$$[T_e] = \begin{bmatrix} 1 & 0 & 0 & 0 & 0 & 0 \\ 0 & \cos(\theta) & \sin(\theta) & 0 & 0 & 0 \\ 0 & -\sin(\theta) & \cos(\theta) & 0 & 0 & 0 \\ 0 & 0 & 0 & 1 & 0 & 0 \\ 0 & 0 & 0 & 0 & \cos(\theta) & \sin(\theta) \\ 0 & 0 & 0 & 0 & -\sin(\theta) & \cos(\theta) \end{bmatrix}.$$

Using the assembled global co-ordinate transformation matrix, the global stiffness matrix is transformed from the rotating to the stationary co-ordinate system using the following relation:

$$[K]^{s} = [T_g]^{T}[K]^{r}[T_g].$$

The above updated stiffness matrix along with an updated force vector corresponding to the new position of the rotor are then used to reevaluate the response of the rotor for the next one degree of rotation using Eq. (32). The response along with the new updated stiffness matrix is used to estimate the nodal forces on the crack finite element [Eq. (33)]. The nodal forces in turn are used in estimating the SIF, the sign of which gives amount of crack opening. The stiffness matrix is evaluated and the process is repeated. Thus at every iteration, the overall stiffness matrix of the rotor system is updated by reevaluating the stiffness matrix of the crack finite element. The process of estimating response continues till the difference between the response for a cycle of rotation and that for its previous cycle is within a reasonably low tolerance value (0.1%). Response data is stored for each degree of rotation.

The breathing model described in this section gives a continuous and more realistic variation of stiffness compared to the open crack model used previously in literature. The model forms a strong foundation for study of coupling of vibrations between bending, longitudinal and torsional vibrations in a cracked rotor.

4. Coupling of bending and torsional vibrations

To establish coupling of bending and torsional vibrations, a simply supported rotor–bearing system with a single centrally situated disc of mass 1 kg is considered. A single transverse surface crack is assumed just adjacent to the central disc. The total rotor span is divided into 14 elements of equal length (Fig. 1c). A crack element that has stiffness properties as described in Section 2, is used to represent the crack. Rest of the rotor is modelled with Timoshenko beam elements with six degrees of freedom per node [22]. To start with, unbalance response of an uncracked rotor with and without torsional excitation is estimated. The response is then compared with that of a cracked rotor. The distinguishing features of the response of cracked rotor from the point of view of crack diagnosis are discussed.

The relevant natural frequencies obtained from the eigenvalue analysis of the rotor are as follows:

Uncracked rotor, bending: 221 rad/s and torsional: 790 rad/s.

Cracked rotor ($\bar{a} = 0.4$), bending: 208 and 216 rad/s and torsional: 778 rad/s. It may be noted that for the cracked rotor, the natural frequencies are evaluated based on the reduced stiffness corresponding to fully open crack state (neglecting the breathing of crack) in order to ascertain extent of drop in the natural frequency.

Since the breathing of crack causes a continuous response-dependent change in the stiffness matrix of the crack element, the Newmark method of direct numerical integration is used to estimate the response. The unbalance eccentricity of 1.6e-5 m is assumed. The rotor rotates at 22 rad/s, which is approximately 1/10th of bending critical speed.

Initially an unbalance response of the uncracked rotor is determined. Figs. 5a and c show the time domain response and Figs. 5b and d show the corresponding frequency spectra in the vertical and horizontal directions showing only rotational frequency of vibration with absence of any higher harmonic frequencies. No torsional response was observed in this case (hence not shown in the figure).

Next, a torsional excitation of $100\sin(221t)$ N m is applied at the first node of the uncracked rotor in addition to unbalance excitation at the disc location. The response obtained is shown in

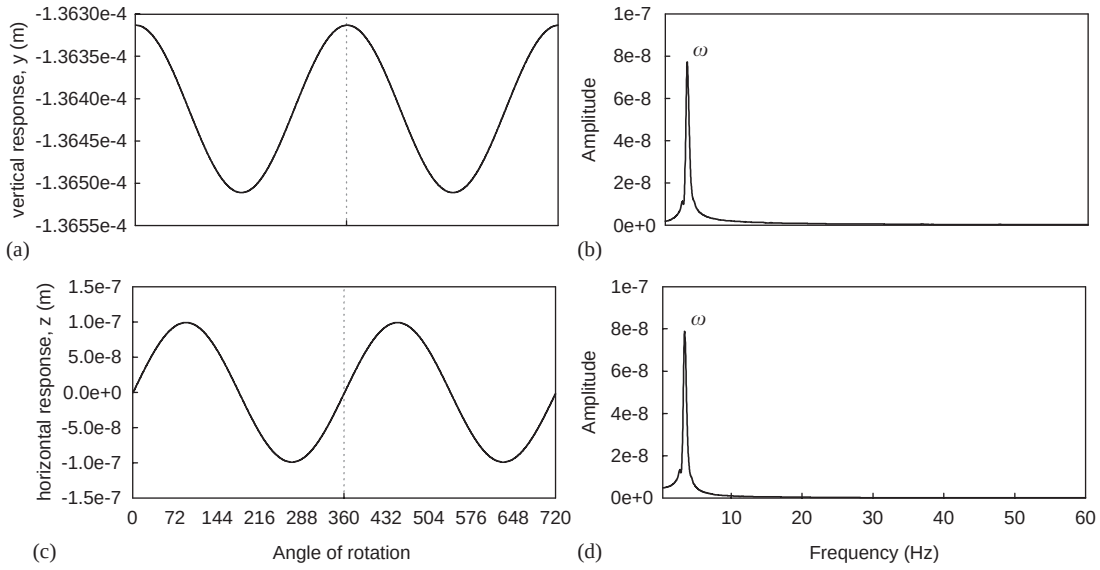

Fig. 5. Unbalance response of an uncracked rotor without torsional excitation. (a) and (b) Response in vertical direction; (c) and (d) response in horizontal direction; $\omega = 1/10\omega_0$.

Fig. 6. From Figs. 6a–d, it may be noted that the frequency content and the amplitudes of vibration in lateral directions show negligible change with the given torsional excitation. However, the response in the torsional mode of vibration shows torsional excitation frequency of 35 Hz (Fig. 6f). The torsional excitation is applied to check if this excitation generates any response in the lateral vibration due to coupling of torsional and lateral bending vibrations. Due to absence of any coupling mechanism in an uncracked shaft, the torsional excitation fails to generate any response in bending mode of rotor vibration (Figs. 6b and d).

The response of a cracked rotor is now studied under similar excitation conditions (unbalance and unbalance with torsional harmonic excitation). The unbalance response of a cracked rotor with crack depth ratio of $\bar{a} = 0.3$ is shown in Fig. 7. No torsional or axial excitation is applied to the system in this case. The lateral vibrations in both vertical and horizontal directions (Figs. 7b and d) contain 1st, 2nd and 3rd harmonic of rotational frequency. Similarly, the longitudinal and torsional vibration spectra (Figs. 7f and h) show first two harmonics, the torsional vibration spectra also show 4th harmonic. The existence of rotational frequency and its higher harmonics in the torsional vibration spectrum without any explicit torsional excitation does indicate an existence of a prominent coupling mechanism. The unbalance excitation in lateral direction generates torsional vibrations in the cracked rotor. Similarly, the axial vibration response also indicates the rotational frequency and its second harmonic (Figs. 7e and f). These frequency components in the axial vibration in the absence of any external axial excitation are indicative of a coupling mechanism between bending and longitudinal vibrations. The results shown in Fig. 7 thus indicate the coupling phenomenon between the bending and the torsional vibrations as well as between the bending and the longitudinal vibrations.

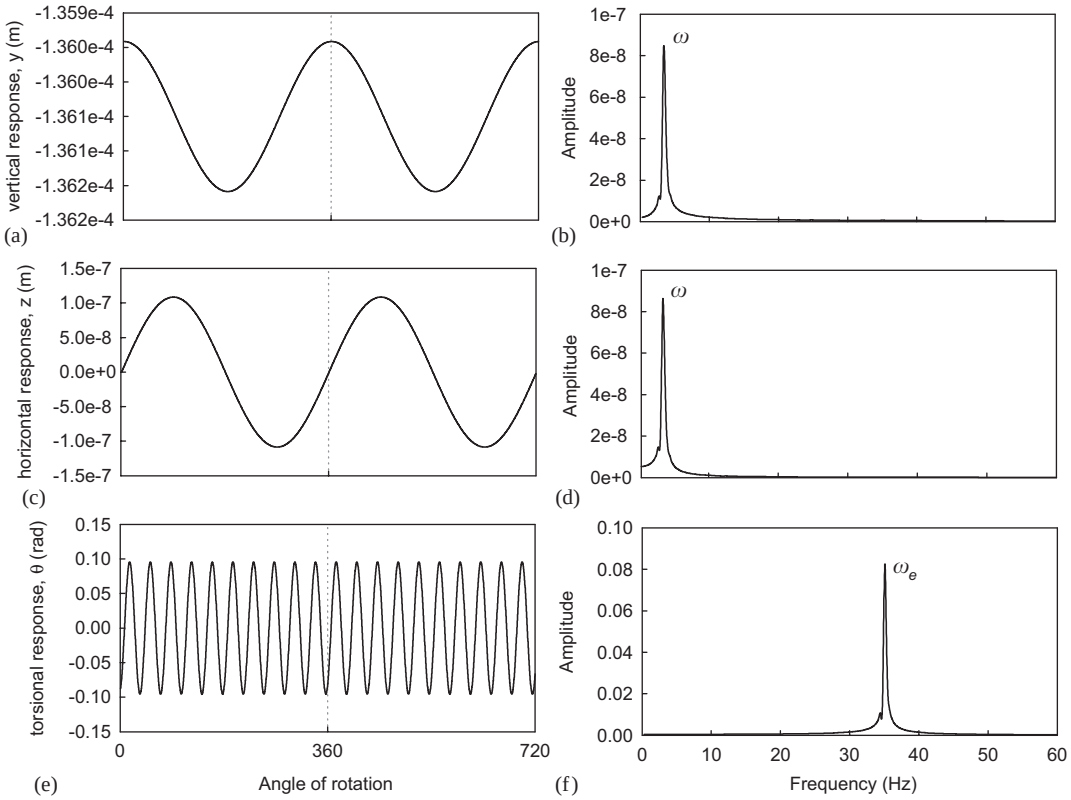

Fig. 6. Unbalance response of an uncracked rotor with torsional excitation; $\omega_e = \omega_0$, $\omega = 1/10\omega_0$. (a) and (b) Response in vertical direction; (c) and (d) response in horizontal direction; (e) and (f) torsional response.

In order to enhance the signals in all these spectra and to explore further the coupling phenomenon due to crack, a harmonic torsional excitation ($100\sin(\omega_e t)$) is applied at node 1 of the FE model. The torsional excitation is in addition to the unbalance excitation in the lateral direction at the disc location. The coupling of longitudinal, bending and torsional vibrations is already indicated in the previous case of unbalance excitation (Fig. 7). In the present case, the frequency of torsional excitation ω_e is tuned to the bending natural frequency of the system (ω_0).

The purpose of such excitation is to excite the system torsionally with a frequency that has relevance in the lateral mode of vibration of the rotor and then check if this excitation generates resonance in the bending vibration of the rotor. With this excitation, if the bending natural frequency is prominently observed in the lateral vibration spectrum, it would indicate a coupling mechanism between torsional and bending vibration in the rotor. Since in the present rotor-bearing system no other coupling mechanism is considered, the response would eventually establish the presence of crack in the rotor. Hence the torsional excitation as mentioned above is applied. The crack depth ratio considered is $\bar{a} = 0.3$ and the rotational speed of the rotor is 22 rad/s (3.5 Hz), which is 1/10th of the bending natural frequency of the uncracked rotor (35 Hz). The time domain and frequency domain signals are shown in Fig. 8. The time domain signal for two

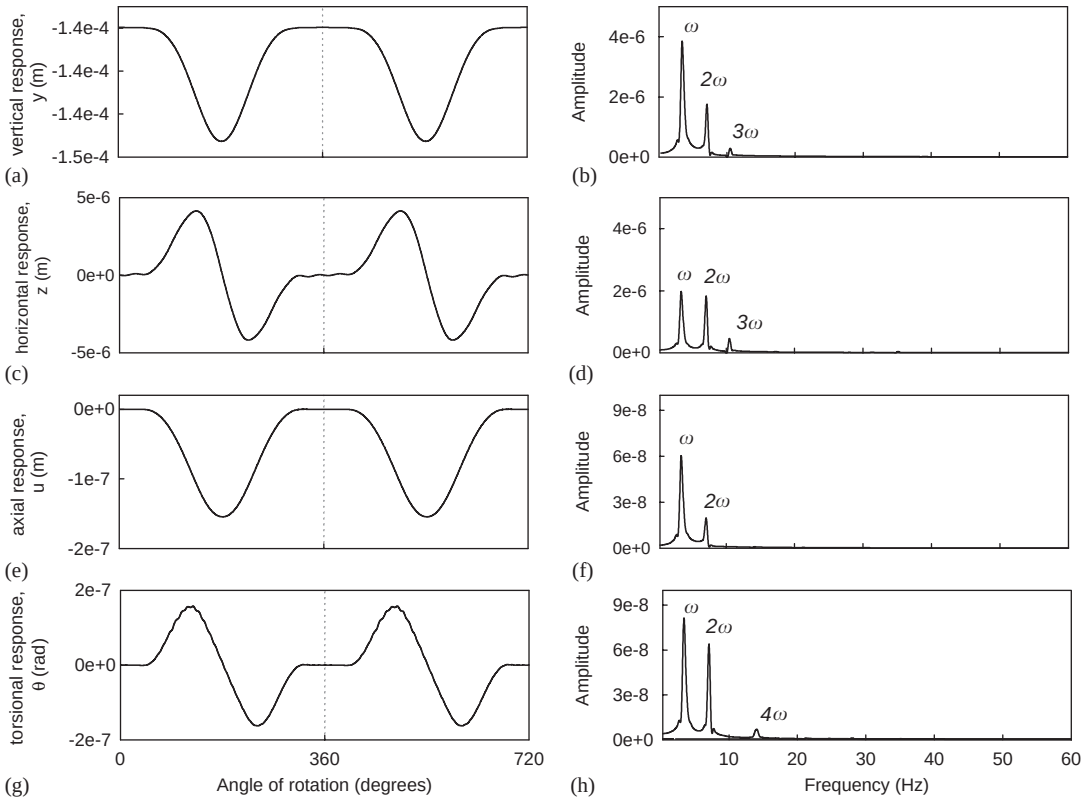

Fig. 7. Unbalance response of the cracked rotor ($\bar{a} = 0.3$) without torsional excitation ($\omega = 22$ rad/s).

cycles of rotation in horizontal and vertical directions (Figs. 8a and c) show apparent presence of torsional excitation frequency (35 Hz) along with a low rotational frequency component ($\omega = 3.5$ Hz). These time domain signals show beating phenomenon. The spectrum in vertical direction (Fig. 8b) show first three harmonics of the rotational frequency and also the bending natural frequency (ω_0) that equals the torsional excitation frequency (ω_e) The frequency ω_0 is flanked by side bands separated by rotational frequency (ω). The amplitude of bending natural frequency shows a substantial difference in the two directions. The ω_0 frequency component is 1.7e-5 in the horizontal direction (Fig. 8d) compared to 5.7e-6 in the vertical direction (Fig. 8b) i.e., more than 3 times stronger in the horizontal direction. The rotational frequency and its harmonics modulate the torsional excitation frequency. The interaction of the torsional excitation frequency with the rotational frequency and its harmonics leads to the appearance of sum and difference frequencies ($\omega_e \pm m\omega$) around the bending natural frequency.

Considering the axial vibration time domain signal without torsional excitation (Fig. 7e), the application of torsional harmonic excitation brings about a distinctive change in the signal (Fig. 8e). The presence of high-frequency components is seen in the time domain signal that is confirmed in the frequency spectrum (Fig. 8f). The spectrum shows sidebands ($\omega_0 \pm \omega$ and $\omega_0 \pm 2\omega$) around the bending natural frequency (ω_0). Although small in amplitude, these sum and

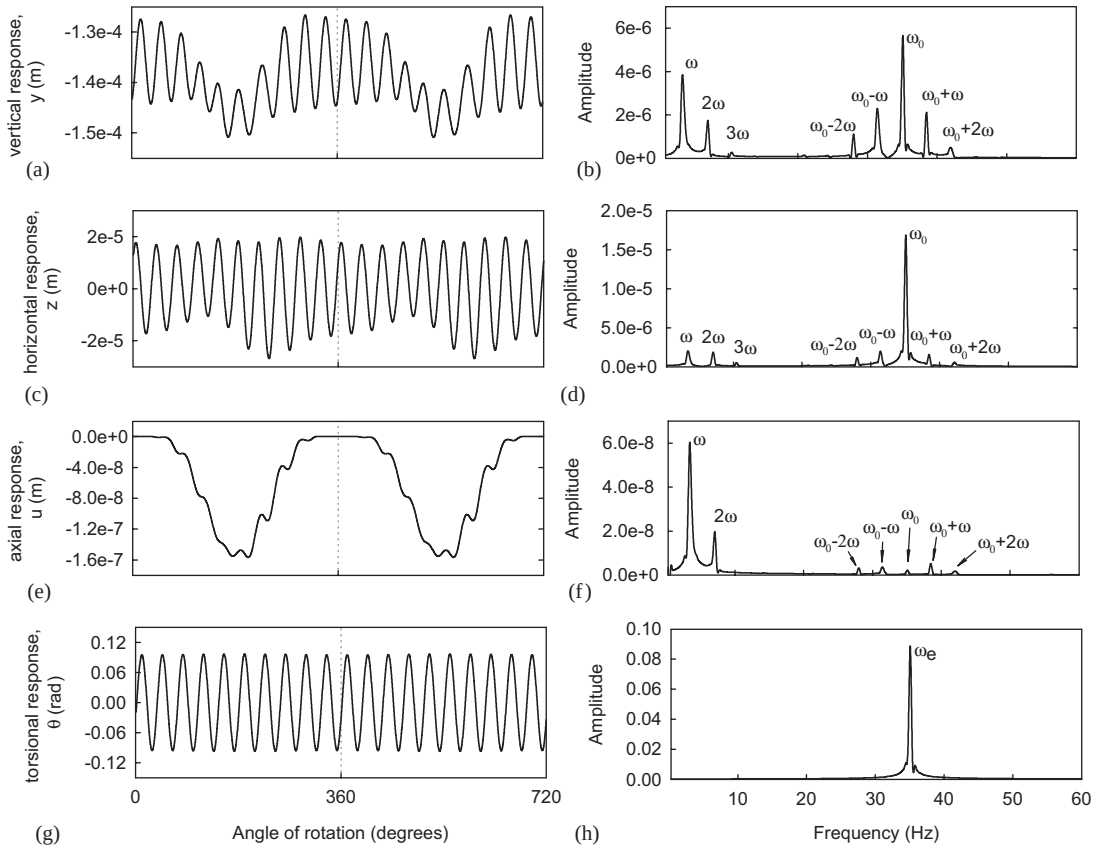

Fig. 8. Unbalance response of a cracked rotor ($a/D=0.3$) with torsional excitation; $\omega_e=\omega_0$ and $\omega=22$ rad/s.

difference frequencies in the longitudinal spectrum indicate a coupling between lateral and longitudinal vibrations as these frequencies are observed in the bending vibration spectrum. It may be noted that there is no longitudinal excitation given to the cracked rotor.

The presence of bending natural frequency in the lateral vibration spectrum under the torsional harmonic excitation is an indication of the presence of transverse crack in the rotor. The stronger bending natural frequency component in the horizontal direction than in the vertical direction that is observed here is also an important crack signature.

The sensitivity of these frequencies observed in the lateral vibration spectrum due to the torsional harmonic excitation to the crack depth is shown in Fig. 9. The figure shows that the bending natural frequency component is more sensitive in horizontal direction than in vertical direction. The variation of amplitude of this frequency component is non-linear. The increase in the amplitudes of other frequency components is marginal as compared to the natural frequency component in the horizontal direction. The frequency of interest ω_0 that indicates the coupling between torsional and lateral vibrations and hence the presence of crack, is highly sensitive to the crack depth.

Next, the harmonic torsional excitation is applied to the cracked rotor rotating at a speed that is not equal to integer fraction of bending critical speed. In this case, $\omega=27$ rad/s (4.3 Hz)

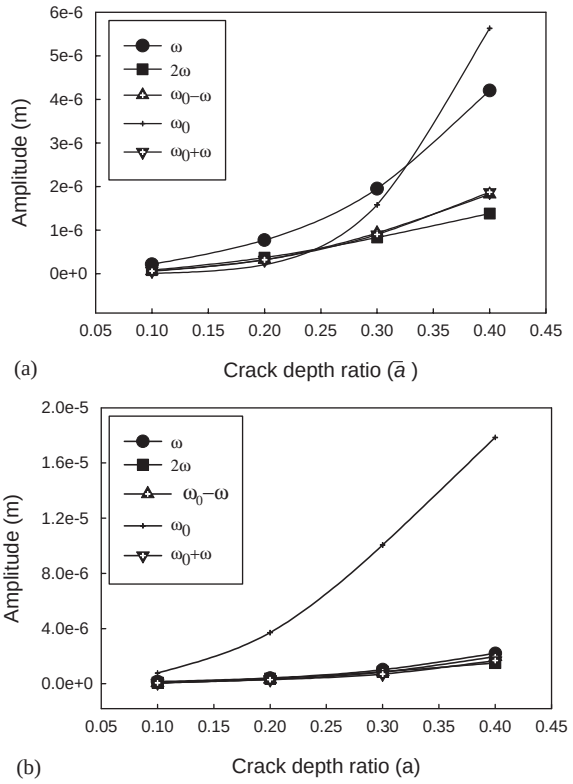

Fig. 9. Variation of amplitudes of various frequency components with crack depth ratio in (a) vertical and (b) horizontal response.

and harmonic torsional excitation is with frequency 120 rad/s (19 Hz). Thus neither the higher harmonics of the rotational frequency nor the torsional excitation frequency match with the bending natural frequency (35 Hz). Therefore in the lateral vibration spectra shown in Figs. 10b and d, the bending natural frequency ω_0 is not seen. Instead the torsional excitation frequency ω_e and side frequencies around ω_e namely, $\omega_e \pm \omega$ and $\omega_e \pm 2\omega$ are seen. The spectra show the rotational frequency and its higher harmonics due to the non-linearity of crack. The side frequencies are present due to interaction between torsional excitation frequency and the lateral rotational frequency and its harmonics as explained earlier. These lateral vibration spectra (Figs. 10b and d) show some frequency components (sum and difference frequencies around the torsional excitation frequency) that are not harmonics of rotational frequencies. These frequencies are due to the coupling between the torsional and lateral vibrations and hence indicate the presence of crack in the rotor.

The sum and difference frequencies that were observed in the previous case (Fig. 10f) are not observed in the longitudinal vibration spectrum here (Fig. 10f). It may be noted that the sum and difference frequencies in the bending vibration spectra, which can appear in the longitudinal spectrum due to coupling phenomenon, are lower order of magnitude (5e-7 in Figs. 10b and d compared to 2e-6 in Figs. 8b and d).

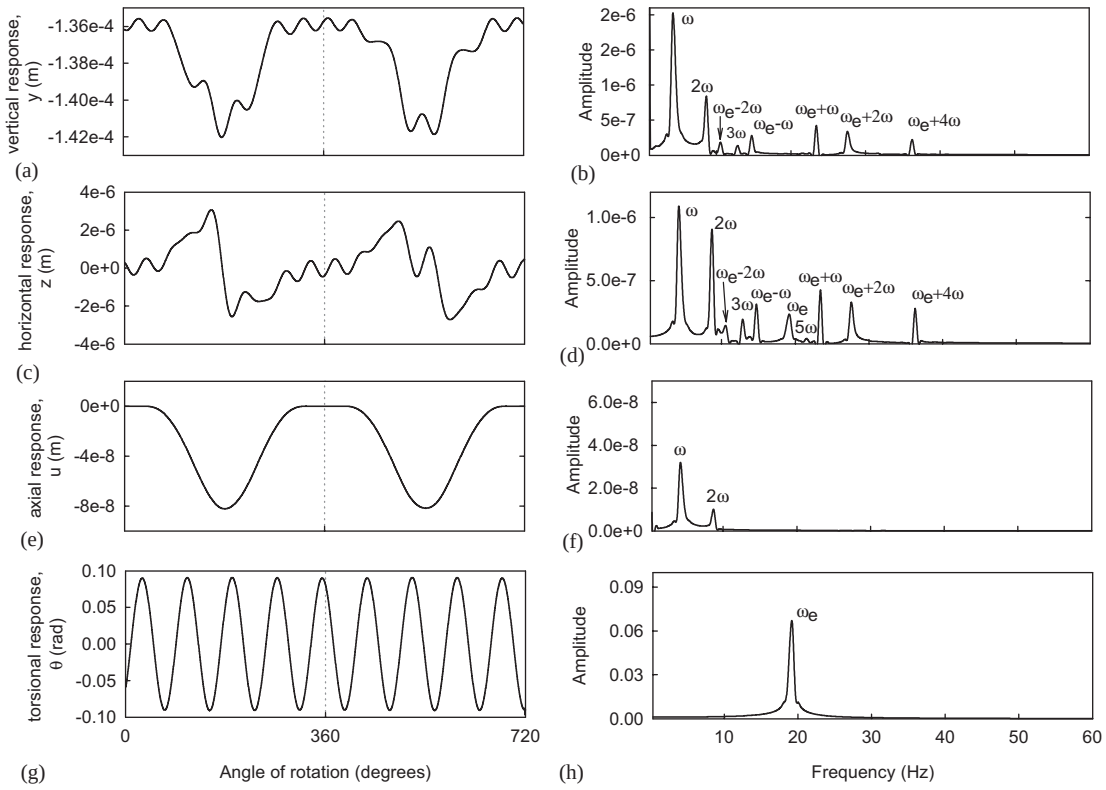

Fig. 10. Unbalance response of a cracked rotor ($\bar{a} = 0.3$) with torsional excitation; $\omega_e = 120$ rad/s and $\omega = 27$ rad/s.

5. Coupling of longitudinal and torsional vibrations

The coupling of torsional and bending vibrations in the cracked rotor under the torsional and unbalance excitations has been investigated in the previous section. In this section, the coupling between torsional and longitudinal vibrations is studied under the axial impulse excitation. Simulations in the previous section have indicated that an additional external excitation is necessary to reveal crack related features in the vibration response. It may be noted that the vibrations with reasonable amplitudes are usually seen when resonance condition is effected in the mode concerned. Darpe et al. [19] have shown that the axial impulses can be used to excite vibrations in the bending mode. In this section the axial excitation in the form of periodic impulses has been used to excite vibrations in the torsional mode in order to exploit the coupling between longitudinal and torsional vibrations. Vibration spectra in all the three modes, namely bending, longitudinal and torsional, are presented for various cases.

To start with, unbalance response of the cracked rotor with $\bar{a} = 0.4$ is investigated without any external axial excitation to ascertain the frequency content of the rotor's unbalance response. The rotational speed is 1/10th of the fundamental natural frequency in torsional mode and the unbalance eccentricity of 1.6e-5 m is considered. The Newmark method of direct numerical integration is used to estimate the response considering the response-dependent breathing model

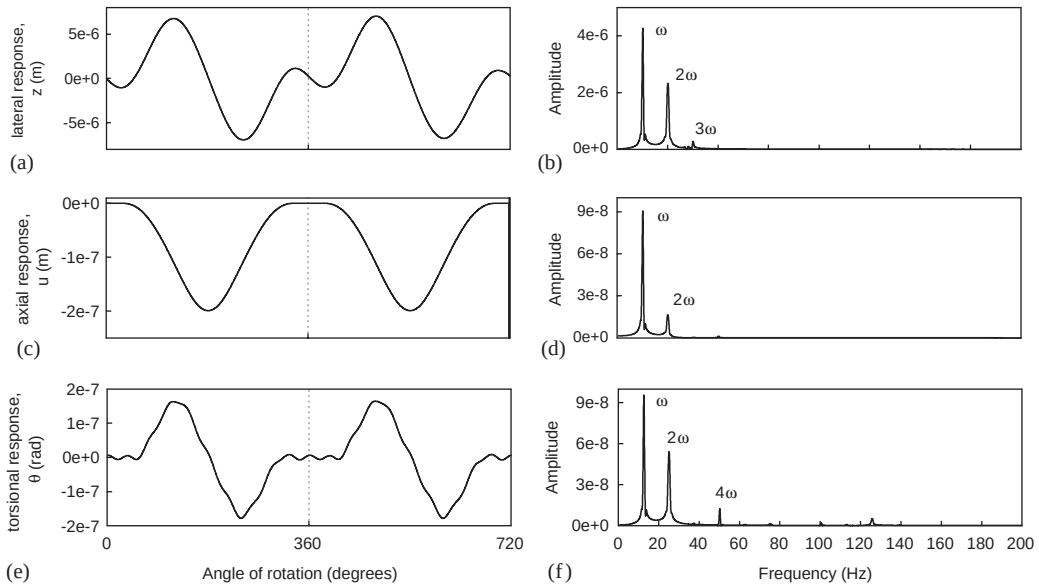

Fig. 11. Unbalance response of a cracked rotor ($\bar{a} = 0.4$) without axial impulse excitation ($\omega = 79$ rad/s).

as discussed in the earlier section. Fig. 11 shows time and frequency domain response of the cracked rotor wherein apart from the first few harmonics of the rotational frequency, the lateral vibration spectra (Fig. 11b) do not show any other frequency components. These lateral vibration frequencies also appear in longitudinal and torsional vibration spectra as shown in Figs. 11d and f respectively. This is despite the absence of any excitation in longitudinal and torsional modes, thus indicating a coupling mechanism between bending and longitudinal and also between bending and torsional vibration.

Next, the cracked rotor is subjected to axial impulses. The axial velocity of the end node is suddenly reduced to simulate application of an impulse. For single axial impulse per rotation, the axial velocity is decreased (by 2 m/s) when the rotor is in reference position i.e., $\theta = 0^\circ$, whereas for multiple impulses, the change of velocity is effected after every $360/i$ degree of rotation, i being the number of impulses per rotation. Application of a single impulse per rotation has not changed the response of cracked rotor substantially, except in longitudinal direction and hence is not presented here.

However, when several impulses (e.g., four impulses per rotation) are applied, the spectrum of torsional vibration shows noticeable changes (Fig. 12d). The spectrum shows the impulse excitation frequency (ω_I) and its harmonics ($n\omega_I$). Due to interaction of these excitation frequencies ($n\omega_I$) with the rotational frequency and its harmonics ($m\omega$), the sum and difference frequencies ($n\omega_I \pm m\omega$) are observed around the excitation frequencies ($n\omega_I$). The natural frequency of torsional vibration (125.7 Hz) is also prominently seen in the spectrum. It may be noted that the frequency component $2\omega_I + 2\omega$ matches with the torsional natural frequency. Because of the presence of these frequencies, the time domain signal of torsional vibration (Fig. 12c) shows considerable change compared to the unexcited case (Fig. 11e).

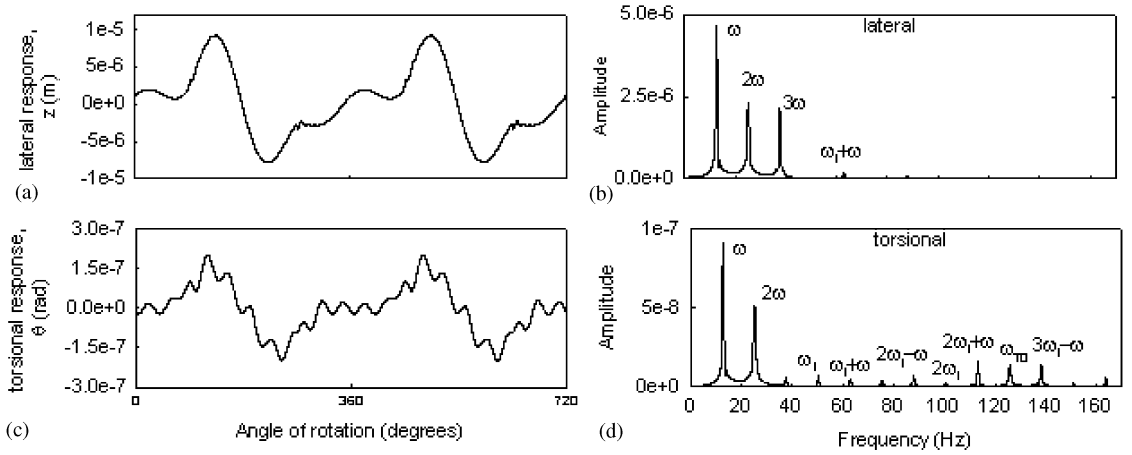

Fig. 12. Unbalance response of a cracked rotor ($\bar{a} = 0.4$) with axial impulse excitation (four impulses per rotation); $\omega_I = 50.3$ Hz, $\omega = 12.6$ Hz.

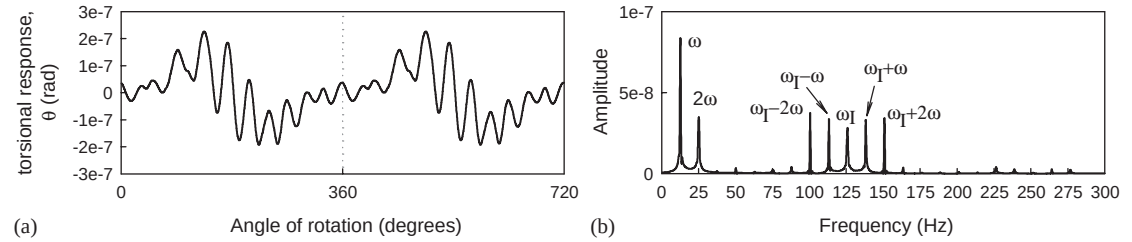

Fig. 13. Unbalance response of a cracked rotor ($\bar{a} = 0.4$) with axial impulse excitation (10 impulses per rotation); $\omega_I = 125.7$ Hz, $\omega = 12.6$ Hz.

The presence of rotational frequency and its harmonics in the torsional vibration indicate the coupling between the lateral and torsional vibration as these frequencies are generated in the bending vibrations due to non-linear effects of the breathing crack under the influence of unbalance and gravity.

The effect of axial excitation shows slight change in the frequency spectrum of the lateral vibration (Fig. 12b), compared to the spectra for unexcited case (Fig. 11b) in the form of stronger third harmonic component (3ω). This is explained from the fact that the 3ω frequency component, which is generated due to the non-linear behaviour of the breathing crack, matches with one of the sum and difference frequencies (ω_I-ω i.e., 37.7 Hz) generated in the lateral vibration due to the axial excitation frequency. Another simulation is carried out in which three axial impulses per rotation ($\omega_I = 3\omega$) are applied to the rotor. The results show a stronger 2ω frequency component compared to the case without any axial excitation. In this case, ω_I-ω frequency component matched with 2ω harmonic frequency.

When the number of impulses are increased to 10 impulses per rotation, the axial impulse excitation frequency ($\omega_I = 125.7$ Hz) matches with the torsional natural frequency (ω_{To}) and hence the amplitude of torsional natural frequency increases considerably (Fig. 13b). The sum and

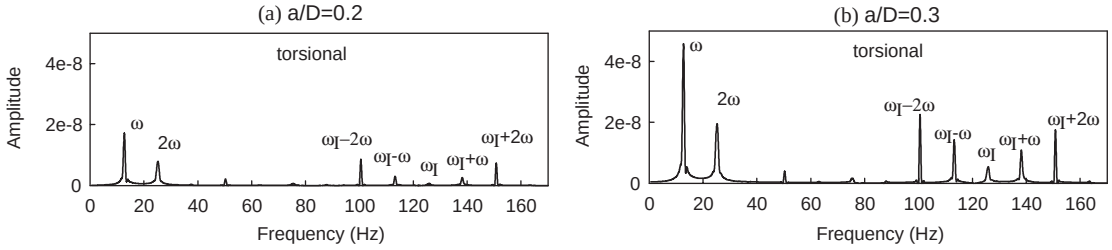

Fig. 14. Unbalance response of a cracked rotor with axial impulse excitation (10 impulses per rotation) showing effect of crack depth; (a) $\bar{a} = 0.2$ and (b) $\bar{a} = 0.3$ ($\omega_I = 125.7$ Hz, $\omega = 12.6$ Hz).

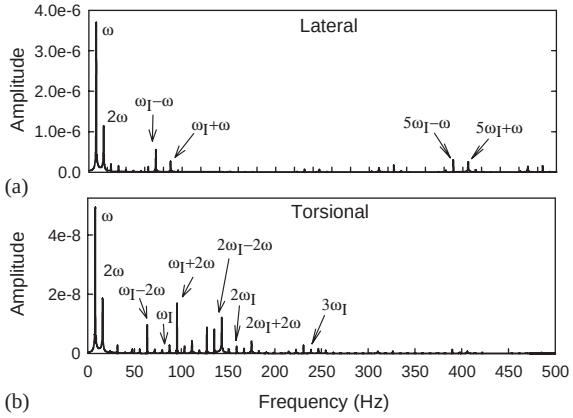

Fig. 15. Unbalance response of a cracked rotor ($\bar{a} = 0.3$) with axial impulse excitation (10 impulses per rotation); $\omega_I = 79.6$ Hz, $\omega = 7.96$ Hz.

difference frequencies ($\omega_I \pm m\omega$) around the impulse excitation frequency are also stronger in amplitude. Traces of sum and difference frequencies ($2\omega_I \pm m\omega$) around the second harmonic of the axial excitation frequency ($2\omega_I$ i.e., 251.5 Hz) are also seen in the spectrum but are very small in amplitude.

When the crack depth ratio is reduced to $\bar{a} = 0.2$, the effect of coupling of vibrations even with such a small crack depth is seen in the torsional vibration spectrum (Fig. 14a) in which the side bands due to interaction between axial and torsional frequencies are seen. Although the torsional natural frequency component for lower crack depth is smaller in amplitude, the side bands around it are quite strong and comparable in amplitude to the rotational frequency and its harmonics. Fig. 14b shows similar response for crack depth of $\bar{a} = 0.3$, where the amplitudes of all the frequency components show noticeable increase, indicating the sensitivity of these frequency components to crack depth.

Response of the cracked rotor rotating at 50 rad/s (7.96 Hz), which is not an integer fraction of the torsional natural frequency, is also studied. The impulse excitation frequency with 10 impulses per rotation is 79.6 Hz, which is different from the torsional natural frequency (125.3 Hz). None of the higher harmonics of rotational frequency (7.96 Hz) matches with the torsional natural frequency. Fig. 15a shows the effect of axial excitation on the lateral vibration response as the

excitation frequency (79.57 Hz) and its harmonics are seen modulated by rotational frequency and its harmonics leading to the presence of side bands around $n\omega_I$ in the lateral vibration response. Although side bands are stronger around ω_I, they are also found stronger around $5\omega_I$ (397.85 Hz). It may be noted that the third natural frequency of bending vibration is 416 Hz for $\bar{a} = 0.3$. Although the second natural frequency of bending vibration (228 Hz) is also closer to one of the harmonics of axial excitation frequency ($3\omega_I = 238.7$ Hz), the side bands around $3\omega_I$ are not as strong as those around $5\omega_I$. However this is expected due to the fact that the crack is positioned near midspan and hence is closer to the node position of the second mode. The response with the crack situated at approximately 1/3rd the span (not shown here) has shown increased amplitude of side bands around $3\omega_I$ frequency.

Although the axial excitation frequency is not explicitly seen in the lateral vibration spectrum, its presence in the spectrum is through the sum and difference frequencies that are produced due to the interaction of the axial excitation frequency and the rotational frequency and its harmonics. It has been shown in Ref. [19] that the axial excitation frequency appears in the lateral vibration when it matches with the bending natural frequency.

The axial excitation frequencies are thus observed in the lateral vibration spectrum (Fig. 15a) and also in the torsional vibration spectrum (Fig. 15b). The sum and difference frequencies in the torsional vibration spectrum are because of the interaction of axial excitation frequencies and the rotational frequency and its harmonics. Since the rotational frequency and its harmonics are due to the unbalance and gravity excitation in the lateral vibration, the presence of these frequencies in the torsional vibration spectrum indicates the coupling between the torsional and lateral vibrations. The frequency spectra in Fig. 15 thus show all the three coupling mechanisms, namely, between longitudinal and lateral vibrations, between longitudinal and torsional vibrations as well as between lateral and torsional vibrations.

6. Conclusions

Coupled longitudinal–bending–torsional vibrations have been studied using the finite element model of a cracked rotor. The stiffness matrix of a Timoshenko beam element with six degrees of freedom per node is modified to account for the presence of crack and then this updated matrix is used to represent the crack. The stiffness matrix accounts for all the coupling mechanisms that are known to exist in a cracked rotor. The coupling is studied with a response-dependent non-linear breathing crack model accounting the partial crack closing. The model is useful in analyzing the response of cracked rotor to any type of excitation encountered in a rotor-bearing system, steady or transient. The crack model thus forms a strong foundation for the study of coupling of vibrations between bending, longitudinal and torsional vibrations in a cracked rotor.

The torsional harmonic excitation and periodic axial impulse excitation to the cracked rotor is used and the response of the cracked rotor in torsional, lateral and axial directions is studied in both time and frequency domain.

When the torsional harmonic excitation with frequency equal to the bending natural frequency is applied to the cracked rotor, bending natural frequency and sum and difference frequencies are observed in the lateral vibration spectrum due to interaction of the torsional excitation frequency with rotational frequency and its harmonics. The presence of bending natural frequency in the

lateral vibration spectrum is shown to be sensitive to the crack depth. The longitudinal vibration spectrum shows the presence of the bending natural frequency and the sum and difference frequencies around it. These results thus establish the coupling between torsion and bending as well as between bending and longitudinal vibrations.

The coupled torsional–longitudinal vibrations of a rotating cracked shaft using breathing crack model have been studied here. Such analysis has not been reported in previous studies. The periodic axial impulses when tuned to the torsional natural frequency excite resonance conditions in the torsional vibrations leading to the presence of the torsional natural frequency flanked by side bands separated by the rotational frequency in the torsional vibration spectrum. Thus the frequency spectrum of torsional vibrations exhibits both the coupling mechanisms; axial–torsional due to presence of axial excitation frequencies and torsional–bending due to the presence of the side bands separated by rotational frequency around axial excitation frequencies. The axial excitation frequencies are present in both the torsional and the bending vibration spectra showing all the coupling mechanisms in one place, namely, axial–bending, axial–torsion and torsion–bending.

The rotor crack diagnosis based on harmonics of rotational frequency like 2x is sometimes unreliable as other faults also generate these frequencies. The frequency spectra presented here for cracked rotors are generally not exhibited by other common faults as most of the faults do not couple the vibrations in bending, longitudinal and torsion. The interaction of external excitation frequencies considered in this study with the rotational frequency and its harmonics of the cracked rotor due to the coupling for a cracked rotor has resulted in interesting and unique frequency patterns that could be very useful from viewpoint of diagnosis of crack. Hence the crack detection based on the response to such excitations could prove to be more reliable as well as convenient since the excitation is applied to the rotating shaft and the rotor is not required to be brought to rest.

Appendix A. Nomenclature

a	depth of crack
D	diameter of the shaft
$\bar{a}$	crack depth ratio (a/D) for crack
l	length of the shaft element containing crack
m	mass of the disc
ε	eccentricity of mass of disc from its geometric centre
θ	angle of rotation of shaft
E	Young's modulus
P_i	nodal forces on the crack element
u_i	displacement along ith co-ordinate
k_ξ, k_η	direct stiffness of the shaft in ξ_1 and η_1 direction respectively
$k_{\xi\eta}$, $k_{\eta\xi}$	cross-coupled stiffnesses
ω	rotational speed in rad/s
ω_e	torsional harmonic excitation frequency
ω_I	axial impulse excitation frequency

ω_0	Bending natural frequency
ω_{To}	torsional natural frequency
t	time in s
$[M]^s$, $[C]^s$, $[K]^s$	mass, damping and stiffness matrix of the rotor system in stationary co-ordinate system
$[K]^r$	stiffness matrix of the rotor system in rotating co-ordinate system
q^s	rotor response in stationary co-ordinate system
q^r	rotor response in rotating co-ordinate system
f^s	forces on the rotor in stationary co-ordinate system

References

[1] A.D. Dimarogonas, C.A. Papadopoulos, Vibration of cracked shafts in bending, Journal of Sound and Vibration 91 (1983) 583–593.

[2] C.A. Papadopoulos, A.D. Dimarogonas, Coupled longitudinal and bending vibrations of a rotating shaft with an open crack, Journal of Sound and Vibration 117 (1987) 81–93.

[3] B. Grabowski, The vibrational behaviour of a rotating shaft containing a transverse crack, in: O. Mahrenholtz (Ed.), Dynamics of Rotors—Stability and System Identification, CISM Courses and Lectures, Vol. 273, Springer, New York, 1984.

[4] R. Gasch, Dynamic behavior of a simple rotor with a cross sectional crack, in: Vibrations in Rotating Machineries—Proceedings of the International Conference, Institution of Mechanical Engineers, 1976, pp. 123–128.

[5] I.W. Mayes, W.G.R. Davies, Analysis of the response of a multi-rotor-bearing system containing a transverse crack in a rotor, Journal of Vibration, Acoustics, Stress, and reliability in Design 106 (1984) 139–145.

[6] H.D. Nelson, C. Nataraj, The dynamics of a rotor system with a cracked shaft, Journal of Vibration, Acoustics, Stress and Reliability in Design 108 (1986) 189–196.

[7] C.A. Papadopoulos, A.D. Dimaragonas, Stability of cracked rotors in the coupled vibration mode, Journal of Vibration, Acoustics, Stress and Reliability in Design 110 (1988) 356–359.

[8] B.K. Schmalhorst, Numerical simulation of cracked rotor's vibrations due to measured crack shapes, in: Proceedings of the Second International Symposium on Transport Phenomena, Dynamics and Design of Rotating Machinery, Vol. 2. Honolulu, HI, 1988, pp. 211–225.

[9] Li. Changhe, O. Bernasconi, N. Xenophontidis, A generalised approach to the dynamics of cracked shafts, Journal of Vibration, Acoustics, Stress and Reliability in Design 111 (1989) 257–263.

[10] J. Wauer, Modeling and formulation of equations of motion for cracked rotating shafts, International Journal of Solids Structures 26 (1990) 901–914.

[11] W.M. Ostachowicz, M. Krawczuk, Coupled torsional and bending vibrations of a rotor with an open crack, Archives of Applied Mechanics 62 (1992) 191–201.

[12] A.S. Sekhar, B.S. Prabhu, Vibration and stress fluctuation in cracked shafts, Journal of Sound and Vibration 169 (1994) 655–667.

[13] O.N.L. Abraham, J.A. Brandon, The modeling of the opening and closure of a crack, Journal of Vibration and Acoustics 117 (1995) 370–377.

[14] C.A. Papadopoulos, A.D. Dimarogonas, Coupling of bending and torsional vibration of a cracked Timoshenko shaft, Ingenieur-Archiv 57 (1987) 257–266.

[15] C.A. Papadopoulos, A.D. Dimarogonas, Coupled longitudinal and bending vibration of a cracked shaft, Journal of Vibration, Acoustics, Stress and Reliability in Design 110 (1988) 1–8.

[16] C.A. Papadopoulos, A.D. Dimarogonas, Coupled vibration of cracked shafts, Journal of Vibration and Acoustics 114 (1992) 461–467.

[17] Muszynska, P. Goldman, D.E. Bently, Torsional/lateral vibration cross-coupled responses due to shaft anisotropy: a new tool in shaft crack detection, in: Vibrations in Rotating Machinery, Institution of Mechanical Engineers Conference Publications, London, 1992, pp. 257–262.
[18] K.R. Collins, R.H. Plaut, J. Wauer, Detection of cracks in rotating Timoshenko shafts using axial impulses, Journal of Vibration and Acoustics 113 (1991) 74–78.
[19] A.K. Darpe, A. Chawla, K. Gupta, Analysis of the response of a cracked Jeffcott rotor to axial excitation, Journal of Sound and Vibration 249 (2002) 429–445.
[20] S. Suherman, R.H. Plaut, Flexural-torsional response of a cracked rotating shaft with a disk during passage through a critical speed, in: S.C. Sinha, R.M. Evan-Ianowski, (Eds.), Dynamics and Vibration of Time-Varying Structures and Systems, DE-Vol. 56, ASME, New York, 1993, pp. 287–293.
[21] K.J. Bathe, Finite Element Procedures, Prentice-Hall of India, New Delhi, 1996.
[22] H.D. Nelson, A finite rotating shaft element using Timoshenko beam theory, ASME Journal of Mechanical Design 102 (1980) 793–803.